Citation:
Wang, K. and El-Mowafy, A. and Rizos, C. 2022. Bridging clock gaps in Mega-Constellation LEO satellites. In Proceedings of the 2022 International Technical Meeting of The Institute of Navigation. 25-27 Jan 2022, Long Beach, California. http://doi.org/10.33012/2022.18246

Bridging Clock Gaps in Mega-Constellation LEO Satellites

Kan Wang, *National Time Service Center, Chinese Academy of Sciences, Xi'an, China; School of Earth and Planetary Sciences, Curtin University, Perth, Australia; University of Chinese Academy of Sciences, Beijing, China*
Ahmed El-Mowafy, *School of Earth and Planetary Sciences, Curtin University, Perth, Australia*
Chris Rizos, *School of Civil and Environmental Engineering, UNSW, Sydney, Australia*

BIOGRAPHY

Kan Wang is Associate Professor at the National Time Service Center, Chinese Academy of Sciences. She received her PhD in GNSS advanced modelling from ETH Zurich in 2016. Her research interests include high-precision GNSS positioning, LEO precise orbit determination and clock determination, SBAS, and integrity monitoring.
Ahmed El-Mowafy is a Professor of Positioning and Navigation, leader of the GNSS research group, and Director of Graduate Research, School of Earth and Planetary Sciences, Curtin University, Australia. He obtained his Ph.D. from the University of Calgary, Canada, in 1995. He has more than 190 publications in precise positioning and navigation using GNSS, quality control, integrity monitoring and estimation theory.
Chris Rizos is an Emeritus Professor, School of Civil & Environmental Engineering, UNSW. Chris is past president of the International Association of Geodesy (IAG), a former member of the Governing Board of the International GNSS Service (IGS), and is currently president-elect of the International Union of Geodesy & Geophysics (IUGG). Chris has been researching the technology and applications of GPS since 1985 and is an author/co-author of over 650 journal and conference papers.

ABSTRACT

In recent years, mega-constellation Low Earth Orbit (LEO) satellites have been proposed as an augmentation to the Global Navigation Satellite System (GNSS) for positioning on the ground, especially for those in measurement environments with limited satellite visibility. The fast geometry change of these LEO satellites also reduces the convergence time of Precise Point Positioning (PPP) techniques. To realize the benefits brought by these LEO satellites, their precise orbits and clocks need to be delivered to users, which would typically be based on processing the GNSS signals collected onboard LEO satellites. Assuming that this will be possible in the future, during data reception, storage and transmission, however, data gaps could exist in the collected GNSS measurements, which would result in gaps in the LEO clock estimates. The transmission of the LEO satellite clock corrections to users could also experience outages. In this study, taking the Ultra-Stable Oscillator (USO) onboard GRACE FO-1 as an example of LEO satellites that has similar operational conditions to the expected LEO mega-constellations, three different models are proposed for bridging clock gaps varying from 1 to 60 minutes. Model A considers its mid- to long-term systematic effects, Model B bridges the gaps using low-order polynomials employing the data near the gap, and Model C exploits the benefits of both Models A and B. Results show that Model A results in larger errors than the other two models for short clock gaps, while Model B could lead to a dramatic increase in the bridging errors for long gaps, e.g., 1h. Applying Model C for the USO on GRACE FO-1, the mean absolute bridging errors (in range) are within 1cm for gaps shorter than 10min, and within 0.2m for gaps not exceeding 1h. Increasing the polynomial degree of Model C from quadratic to cubic can lead to a reduction in the mean absolute bridging errors to mm- to cm-level.

INTRODUCTION

The Global Navigation Satellite System (GNSS)-based positioning augmented by mega-constellation Low Earth Orbit (LEO) satellites has become a popular topic in recent years [1-4]. Thousands of LEO satellites, which will form a dense network from altitudes of a few hundred kilometres to over 1000km in the near future, would significantly increase the satellite visibility and thus improve the measurement geometry for ground-based positioning users. These improvements would be especially meaningful for

users operating in difficult measurement environments, e.g., in "urban canyon" areas, the bottom of open pit mines, etc. In addition to the improved measurement geometry, due to the low altitudes of the LEO satellites compared to GNSS satellites at Medium Earth Orbit (MEO) or even the Geostationary Orbit (GEO), the signal strength of LEO satellite transmissions will be much higher than those of GNSS satellites, e.g., 300 to 2400 times higher for the LEO satellites Iridium [5]. This could enable the positioning in deep signal attenuation areas, e.g., high-density urban areas, or even in some indoor areas. Besides, the LEO satellite signals are shown to be more resilient to jamming [1] and the fast satellite-to-ground speed whitens the multipath effects [6], which have been a significant bottleneck in the development of high positioning accuracy techniques in complicated measurement environments such as urban areas. The higher (relative to ground) speed of LEO satellites compared to GNSS satellites also results in a rapid change in the measurement geometry. This is essential to resolving the carrier-phase ambiguities and shorten the convergence time for Precise Point Positioning (PPP) techniques from tens of minutes to only a few minutes [7-8].

To realize all the advantages mentioned above in the field of Positioning, Navigation and Timing (PNT), especially for applications having high accuracy requirements that take advantage of the PPP techniques, the use of high-accuracy LEO orbit and clock information is an indispensable condition. Benefiting from their altitudes, the LEO satellites can serve as GNSS "users" at the same time as they are treated as signal transmitters for ground-based PNT users. With GNSS receivers equipped onboard, the precise orbits and clocks of LEO satellites can be determined using appropriate GNSS measurement processing techniques. Without the influences of the tropospheric delays and the complicated multipath effects on the ground, combining undifferenced GNSS signals and dynamic models, LEO Precise Orbit Determination (POD) in the so-called "reduced-dynamic mode" can achieve positional accuracy of centimetres [9-11]. At the same time, high-precision LEO satellite clock estimates at a similar accuracy level can also be obtained [12]. With the signal receiver and transmitter synchronized by the same clock [13], the estimated LEO satellite clocks can be used for LEO-augmented ground-based positioning, when not considering the hardware delays in between the time of the signal reception of GNSS measurements and transmission of LEO satellite's signals. These hardware delays could have uncalibrated variations and this will be further investigated. For the moment they can be treated as time-constant terms [13], which can be absorbed by the estimated float ambiguities of the ground positioning users.

Similar to the GNSS orbits and clocks, the LEO products can have different transmission modes. Nowadays, high-precision GNSS products can be transmitted to users via the Internet or satellite links through, e.g., GEO satellites or even GNSS satellites. For the former case, diverse real-time GNSS services such as the International GNSS Service (IGS) Real-Time Service (RTS) [14-16] and the real-time service provided by the National Centre for Space Studies (CNES) in France [17] are good examples. For the latter case, satellite-broadcast precise GNSS products like those from the Multi-GNSS Advanced Demonstration of Orbit and Clock Analysis (MADOCA) service of the Japanese Quasi-Zenith Satellite System (QZSS) and those from the Australian/New Zealand (AU/NZ) second generation Satellite Based Augmentation System (SBAS) will also find more applications in the future. In a similar manner, high-precision LEO orbit and clock information can be processed on the ground and transmitted to users via the Internet or via satellite links. However, in addition to the signal outages due to problems of transmission or signal blockage in difficult measurement environments [18], the operators of LEO satellites for PNT users face new challenges in generating and providing continuous high-precision products. Due to the much lower altitude of the LEO satellites compared to the GNSS satellites, i.e., from about 300 to 1500km [19], the sub-satellite footprint of an LEO satellite is very limited. Figure 1 shows the area in which the LEO satellite GRACE FO-1 (with an altitude of about 500km) is visible on August 14, 2018, at 10:30 GPS Time (GPST). With an elevation cut-off angle of 5 degrees, the range of the latitude and longitude of this area only amounts to about 36 to 37 degrees. This could be a problem for, e.g., users in remote areas or on the ocean, for which their visible LEO satellites are not visible by any ground reference stations, and the onboard GNSS measurements cannot be transferred and processed on the ground in real-time. Inter-satellite links could be a solution to this problem. Bridging the gaps in the high-precision LEO products could thus be essential for LEO-augmented positioning service in near-real-time, or even for post-processing mode users.

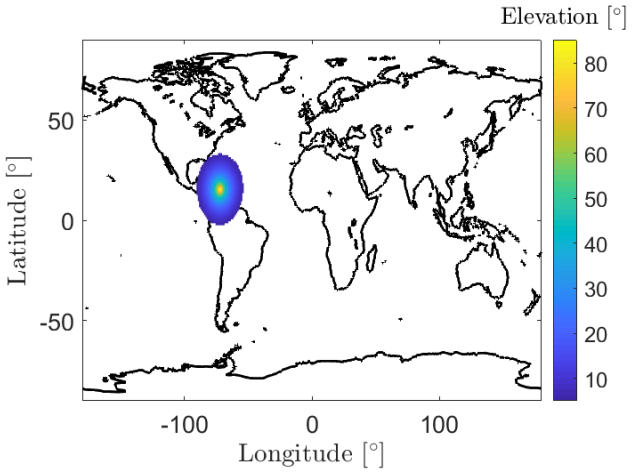

Figure 1. The ground area able to observe the LEO satellite GRACE FO-1 on August 14, 2018, at 10:30 GPST. The elevation angle refers to that from the corresponding ground point to the satellite with a cut-off angle of 5 degrees.

Bridging the gaps in the LEO orbital products would not be a significant problem as adequate dynamic models exist for LEO satellites. As shown in [20], even in cases when the GNSS measurements are not continuously available, i.e., with duty cycles (i.e. the percentage of the period when GNSS is operable) lower than 100%, the orbital accuracy can still reach the level of a few centimetres when high-precision GNSS products are available. For the LEO satellite clock estimates, however, the situation is different. The clock errors are generally not estimated with a strong and long-term model due to the lower stability of the clocks onboard LEO satellites. They are typically estimated as independent epoch parameters [21], or short-term models applied when good clocks are used [22]. The determination of the LEO satellite clock errors to high precision is thus dependent on the GNSS measurements at the corresponding epochs, which can provide results even though the randomness of the clock errors is difficult to model. In case GNSS measurements are not available during a certain period, the estimates of the time series of LEO satellite clock errors would then need to be bridged somehow using the deterministic characteristics of the onboard LEO satellite clocks, such as Ultra-Stable Oscillators (USOs).

In this study, the focus is on bridging the clock error gaps of the USOs, a type of frequency oscillator having good short-term stabilities [22-23] used on LEO satellites of a few scientific missions, e.g., GRACE [24], GRACE Follow-On [25], and Sentinel-3B [26]. In addition to the stochastic and deterministic behaviours of the frequency oscillator itself and the noise introduced by GNSS estimation, systematic effects due to external sources also need to be considered. In this contribution, the strategy for measurement processing for LEO satellite clock estimation is first introduced. It is followed by an analysis of the clock estimates of the LEO satellite GRACE FO-1 as an example with the models for bridging the clock gaps. Finally, the bridging errors are assessed for different models and gap lengths. The conclusion is given at the end of the paper.

PROCESSING OF LEO SATELLITE CLOCKS

The LEO satellite clock errors are estimated in a least-squares adjustment together with the reduced-dynamic POD parameters. The a priori LEO satellite clock synchronization (with the GPS satellite clocks) is performed using the L1 and L2 GPS code measurements after forming the Ionosphere-Free (IF) combination. After pre-processing for outlier removal and cycle slip detection, the IF GPS phase and code observations are used to estimate the LEO satellite clock errors ΔT_{L}, the float ambiguities N_{IF}^{s}, and the orbital parameters:

$$\mathrm{E}(\Delta\phi_{\mathrm{IF}}^{s}) = A_{\mathrm{K}}^{s}\,p_{\mathrm{K}} + A_{\mathrm{D}}^{s}\,p_{\mathrm{D}} + A_{\mathrm{a}}^{s}\,p_{\mathrm{a}} + \underbrace{\Delta t_{\mathrm{L}} + d_{\mathrm{L,IF}}}_{\Delta T_{\mathrm{L}}} + \lambda_{\mathrm{IF}}\,\underbrace{\left(n_{\mathrm{IF}}^{s} + \left(\xi_{\mathrm{L,IF}} - \xi_{\mathrm{IF}}^{s} - d_{\mathrm{L,IF}} + d_{\mathrm{IF}}^{s}\right)/\lambda_{\mathrm{IF}}\right)}_{N_{\mathrm{IF}}^{s}} \tag{1}$$

$$\mathrm{E}(\Delta P_{\mathrm{IF}}^{s}) = A_{\mathrm{K}}^{s}\,p_{\mathrm{K}} + A_{\mathrm{D}}^{s}\,p_{\mathrm{D}} + A_{\mathrm{a}}^{s}\,p_{\mathrm{a}} + \underbrace{\Delta t_{\mathrm{L}} + d_{\mathrm{L,IF}}}_{\Delta T_{\mathrm{L}}} \tag{2}$$

where $\Delta\phi_{\mathrm{IF}}^{s}$ and $\Delta P_{\mathrm{IF}}^{s}$ denote the IF phase and the code "Observed-minus-Computed" (O-C) terms for GPS satellite s, respectively. E(·) is the expectation operator. p_{K}, p_{D} and p_{a} are the six Keplerian elements at the initial state, the 3-dimensional (3D) time-constant orbital dynamic parameters, and the time-constant stochastic accelerations, respectively. The stochastic accelerations are estimated in 6min intervals and are constrained to zeros with a standard deviation of 5×10^{-9} m/s^2. Correspondingly, A_{K}^{s}, A_{D}^{s} and A_{a}^{s} are the partial derivatives of the observations from satellite s with respect to p_{K}, p_{D} and p_{a}, respectively. The estimable LEO satellite clock ΔT_{L} contains, in addition to the LEO satellite clock error Δt_{L}, the IF LEO satellite code bias $d_{\mathrm{L,IF}}$. The estimable float ambiguity N_{IF}^{s} comprises, in addition to the IF float ambiguity term n_{IF}^{s}, the IF LEO satellite phase and code biases $\xi_{\mathrm{L,IF}}$ and $d_{\mathrm{L,IF}}$, as well as the GPS satellite phase and code biases ξ_{IF}^{s} and d_{IF}^{s}. In this study, the final GPS orbits and clocks from the Center for Orbit Determination in Europe (CODE) [27] are used to form the O-C terms. The GPS clocks contain the IF GPS code biases of P1 and P2. The forms of the IF wavelength λ_{IF} and the IF float ambiguity n_{IF}^{s} are:

$$\lambda_{\mathrm{IF}} = \frac{c}{f_1+f_2} \tag{3}$$

$$n_{\mathrm{IF}}^{s} = \frac{f_1^2\lambda_1 n_1^s - f_2^2\lambda_2 n_2^s}{c(f_1-f_2)} \tag{4}$$

where c denotes the speed of light. f_j, λ_j and n_j denote the frequency, the wavelength and the ambiguity on frequency j (with $j = 1, 2$), respectively. The estimated LEO satellite clock ΔT_{L} is to be provided to the ground users despite the additional hardware delays between the receiving time of the GNSS signals and the transmission time of the LEO signals. These hardware biases are to be calibrated on the ground, where the uncalibrated part is assumed to be a constant that can be absorbed by the estimable float ambiguity terms of the ground users. The uncalibrated time-variant part caused by, e.g., the environment, is present but is not accounted for in this study.

The reduced-dynamic POD process uses existing dynamic models for LEO satellite. In this study, the spherical harmonic coefficients of EGM2008 [28] up to a degree of 120 are used as the model for the Earth's non-sphericity and non-homogeneous mass distribution. The gravitational attraction of other planets is considered using ephemerides provided by the Jet Propulsion Lab (JPL) [29]. The solid Earth and pole tides are considered following the International Earth Rotation and Reference Systems Service (IERS) conventions 2010 [30], and the ocean tides are modelled with FES2004 [31]. Data of 24h duration, with a sampling interval of 10s, are processed in a batch mode least-squares adjustment. The resulting orbital parameters are used for computing the final Cartesian orbit parameter information during the entire test period via numerical integration [32]. Taking the POD of the LEO satellite GRACE FO-1 on December 1, 2019, as an example, using the orbits produced by the JPL [33] as the reference, the 3-dimensional root-mean-square error (RMSE) of the estimated orbits amounts to about 2cm, which verifies the proposed processing strategy.

CLOCK MODELLING

The estimated LEO satellite USO clocks $\Delta\hat{T}_{\mathrm{L}}$ are referenced to the reference clock in the CODE final clock products, i.e., a H-Maser, which exhibits higher stability than the USOs analysed in this study for an averaging time of 10s and above [22]. As such, the clock bridging investigated for the post-processing mode here, which is mainly related to the deterministic characteristics of the LEO satellite clocks, is in general free from the influences of the time reference. After detrending with a quadratic polynomial, as discussed in [12], LEO satellite USO clocks could exhibit large long-term periodic effects. Figure 2 shows the periodic effects of the satellite clocks for GRACE FO-1 on December 1, 2019. To explain the contents of the different coloured lines in Figure 2, the clock model is given as follows:

$$\mathrm{E}\left(\Delta\hat{T}_{\mathrm{L}}(t_i)\right) = a_0 + a_1(t_i - t_0) + a_2(t_i - t_0)^2 + A_1 \sin\left(\frac{2\pi}{\hat{T}_1}(t_i - t_0) + \varphi_1\right) + A_2 \sin\left(\frac{2\pi}{\hat{T}_2}(t_i - t_0) + \varphi_2\right) \tag{5}$$

with the polynomial coefficients a_0, a_1 and a_2 estimated in the least-squares adjustment with the corresponding estimates denoted as $\hat{a}_0$, $\hat{a}_1$ and $\hat{a}_2$, respectively. The periods $\hat{T}_1$ and $\hat{T}_2$ were estimated separately before the least-squares adjustment of Eq. (5) [12], and amounts to about 11h 57min and 5h 59min, respectively, for the test day. The amplitudes A_1 and A_2 of the periodic effects have their estimates denoted as $\hat{A}_1$ and $\hat{A}_2$, respectively, and the phases φ_1 and φ_2 have their estimates denoted as $\hat{\varphi}_1$ and $\hat{\varphi}_2$. t_i and t_0 denote the time at epoch i and the processing start time, respectively. In Figure 2, the blue and green lines refer to the terms $\delta\hat{T}_1$ and

$\delta\hat{T}_2$ in Eqs. (6) and (7), respectively, which describe the overlapped (6h+12h) and the 6h periodic effects. The red and magenta lines illustrate the two modelled periodic effects with amplitudes $\hat{A}_1$ and $\hat{A}_2$, respectively:

$$\delta\hat{T}_1(t_i) = \Delta\hat{T}_L(t_i) - (\hat{a}_0 + \hat{a}_1(t_i - t_0) + \hat{a}_2(t_i - t_0)^2) \tag{6}$$

$$\delta\hat{T}_2(t_i) = \delta\hat{T}_1(t_i) - \hat{A}_1 \sin\left(\frac{2\pi}{\hat{T}_1}(t_i - t_0) + \hat{\varphi}_1\right) \tag{7}$$

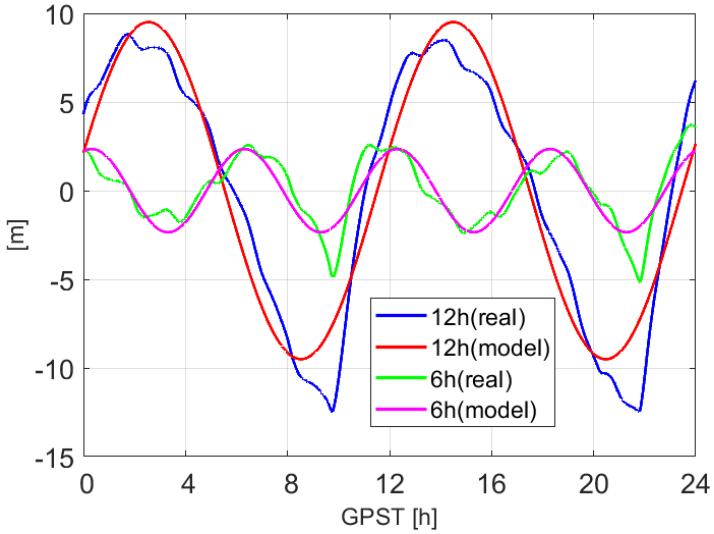

Figure 2. The periodic effects in the clocks of the LEO satellite GRACE FO-1 on December 1, 2019.

From Figure 2 it can be seen that the periodic effects reach several metres and need to be taken into account during clock bridging over long gaps. After detrending with these systematic effects, the remaining clock residuals still contain systematic effects as shown in Figure 3a, which can be represented by the term $\delta\hat{T}_3$:

$$\delta\hat{T}_3(t_i) = \delta\hat{T}_2(t_i) - \hat{A}_2 \sin\left(\frac{2\pi}{\hat{T}_2}(t_i - t_0) + \hat{\varphi}_2\right) \tag{8}$$

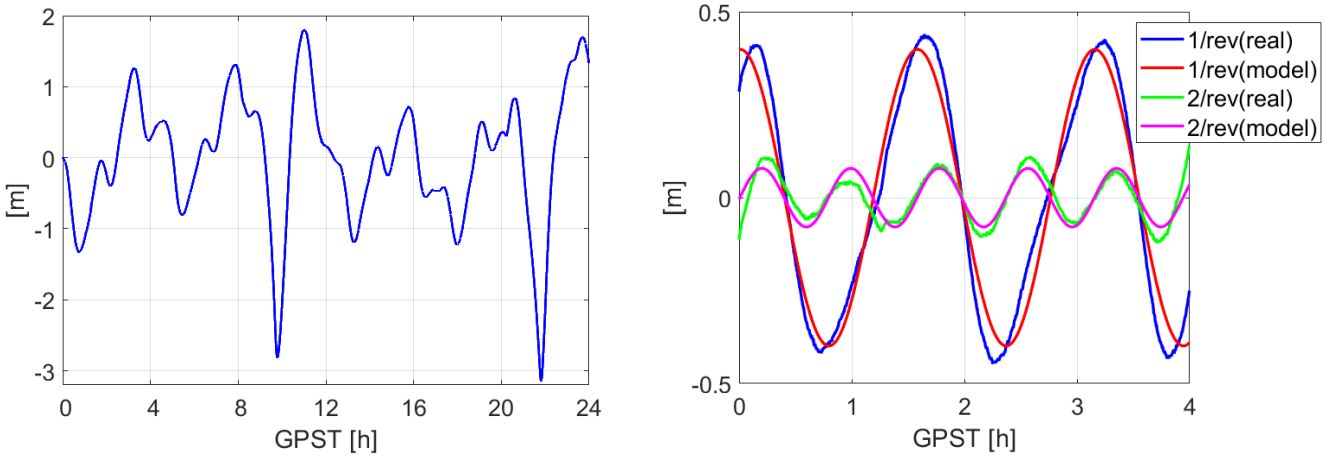

Figure 3. LEO satellite clock residuals (a) after removing the long-term systematic effects (see Eq. (8)) and (b) after further detrending with a fourth-order polynomial over 4h interval. The clock estimates of GRACE FO-1 on December 1, 2019, are used for the plots.

The effects observed in $\delta\hat{T}_3$ (see Figure 3a) are overlapped effects of a high-order polynomial, which could be caused by the mid- and long-term noise behaviour of the USO itself, and the once- and twice-per-revolution (1/rev and 2/rev) terms caused by the more complicated relativistic effects on the LEO satellites, which cannot be perfectly corrected for [34]. After detrending using a fourth-order polynomial (with the polynomial coefficients $b_j, j = 1, \cdots, 4$) for the first 4h of the test day, these 1/rev and 2/rev effects become visible and can be modelled (see Figure 3b). As described in Eq. (9), the LEO orbital period T_L is used for identifying two periodic effects, i.e., the 1/rev effects with the amplitude B_1 and phase ϑ_1, as well as the 2/rev effects with the amplitude B_2 and phase ϑ_2:

$$\mathrm{E}\big(\delta\hat{T}_3(t_i)\big) = b_0 + b_1(t_i - t_0) + \cdots + b_4(t_i - t_0)^4 + B_1 \sin\left(\frac{2\pi}{T_\mathrm{L}}(t_i - t_0) + \vartheta_1\right) + B_2 \sin\left(\frac{4\pi}{T_\mathrm{L}}(t_i - t_0) + \vartheta_2\right) \tag{9}$$

The blue and green lines in Figure 3b correspond to the terms $\delta\hat{T}_4$ and $\delta\hat{T}_5$ (see Eqs. 10 and 11), with the symbol ^ denoting the estimates of the corresponding parameters based on Eq. (9). The red and magenta lines represent the terms $\hat{B}_1 \sin\left(\frac{2\pi}{T_\mathrm{L}}(t_i - t_0) + \hat{\vartheta}_1\right)$ and $\hat{B}_2 \sin\left(\frac{4\pi}{T_\mathrm{L}}(t_i - t_0) + \hat{\vartheta}_2\right)$, respectively:

$$\delta\hat{T}_4(t_i) = \delta\hat{T}_3(t_i) - (\hat{b}_0 + \hat{b}_1(t_i - t_0) + \cdots + \hat{b}_4(t_i - t_0)^4) \tag{10}$$

$$\delta\hat{T}_5(t_i) = \delta\hat{T}_4(t_i) - \hat{B}_1 \sin\left(\frac{2\pi}{T_\mathrm{L}}(t_i - t_0) + \hat{\vartheta}_1\right) \tag{11}$$

After detrending with the modelled clocks in Eq. (9), the remaining clock residuals $\left(\delta\hat{T}_5(t_i) - \hat{B}_2 \sin\left(\frac{4\pi}{T_\mathrm{L}}(t_i - t_0) + \hat{\vartheta}_2\right)\right)$ are at the few centimetre level (see Figure 4), which would remain after the clock bridging. Note that the higher bridging errors could occur since the 1/rev and 2/rev as well as the long-term periodic effects cannot always be perfectly modelled with sinusoidal functions. Some examples will be discussed in the next section.

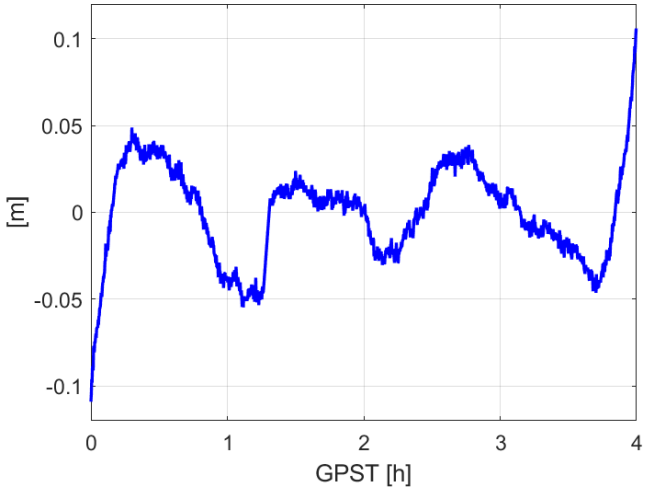

Figure 4. Remaining clock residuals after detrending with the high-order polynomial and the 1/rev and 2/rev periodic effects in Eq. (9).

In general, using available clock estimates within 24h, the long-term systematic effects in Eq. (5) are first modelled with the corresponding polynomial and periodic coefficients estimated. Next, using the clock estimates near the gap with an interval expanding to 4h, a high-order polynomial together with the 1/rev and 2/rev periodic effects are retrieved with Eq. (9). The clock gaps can in this way be merged with $\Delta\check{T}_\mathrm{L}$ based on the models in Eqs. (5) and (9), denoted as Model A with:

$$\Delta\check{T}_\mathrm{A}(t_i) = (\hat{a}_0 + \hat{b}_0) + (\hat{a}_1 + \hat{b}_1)(t_i - t_0) + (\hat{a}_2 + \hat{b}_2)(t_i - t_0)^2 + \hat{b}_3(t_i - t_0)^3 + \hat{b}_4(t_i - t_0)^4 + \sum_{j=1}^{k}\left(\hat{A}_j \sin\left(\frac{2\pi}{\hat{T}_j}(t_i - t_0) + \hat{\varphi}_j\right)\right) + \hat{B}_1 \sin\left(\frac{2\pi}{T_\mathrm{L}}(t_i - t_0) + \hat{\vartheta}_1\right) + \hat{B}_2 \sin\left(\frac{4\pi}{T_\mathrm{L}}(t_i - t_0) + \hat{\vartheta}_2\right) \tag{12}$$

Note that the clock estimates during the gap period are not used to estimate the polynomial and periodic coefficients. As the long-term periodic effects could be satellite-specific, the number of long-term periodic effects is extended from 2 in the case of GRACE FO-1 to k depending on the behaviour of the investigated LEO satellite clocks.

For short clock gaps, merging the gaps simply with a low-order polynomial of degree m using the clock estimates around the gaps may deliver better results. As such, a second model, denoted as Model B, is tested in this study:

$$\Delta\check{T}_{\mathrm{B}}(t_i) = \sum_{j=0}^{m} \hat{c}_j (t_i - t_0)^j \tag{13}$$

where the polynomial coefficients $\hat{c}_j$ are fitted using the clock estimates shortly before and after the gap period. The time window used for estimation of the polynomial coefficients $\hat{c}_j$ is in this study centred at the middle of the clock gap and twice the length of the gap, with the data during the gap period not used.

To explore the benefits from both Models A and B, Model C is developed by first detrending the periodic effects $\Delta\hat{T}_{\mathrm{p}}(t_i)$, and then estimating the polynomial coefficients $\hat{d}_j$ using the data nearby with:

$$\mathrm{E}\left(\Delta\hat{T}_{\mathrm{L}}(t_i) - \Delta\hat{T}_{\mathrm{p}}(t_i)\right) = \sum_{j=0}^{m} \hat{d}_j (t_i - t_0)^j \tag{14}$$

and

$$\Delta\hat{T}_{\mathrm{p}}(t_i) = \sum_{j=1}^{k} \left(\hat{A}_j \sin\left(\frac{2\pi}{\hat{T}_j}(t_i - t_0) + \hat{\varphi}_j\right)\right) + \hat{B}_1 \sin\left(\frac{2\pi}{T_{\mathrm{L}}}(t_i - t_0) + \hat{\vartheta}_1\right) + \hat{B}_2 \sin\left(\frac{4\pi}{T_{\mathrm{L}}}(t_i - t_0) + \hat{\vartheta}_2\right) \tag{15}$$

The bridged clock applying the Model C can in this way be expressed as:

$$\Delta\check{T}_{\mathrm{C}}(t_i) = \sum_{j=0}^{m} \hat{d}_j (t_i - t_0)^j + \Delta\hat{T}_{\mathrm{p}}(t_i) \tag{16}$$

The performance of bridging of the LEO satellite clocks applying the three models will be discussed in the next section.

TEST RESULTS

Based on Models A and B in Eqs. (12) and (13), respectively, the LEO satellite clocks of GRACE FO-1 on December 1, 2019, are used for the tests. Figure 5a shows the real (blue), missing (red) and bridged clocks (green) for a gap of 3min around 2:00 in GPST based on Model A. The plotted clocks are detrended with the polynomials and the mid- to long-term periodic terms (see the detrended part $\Delta\check{T}_{\mathrm{m}}$ in Eq. 17) for the purpose of visualization:

$$\Delta\check{T}_{\mathrm{m}}(t_i) = \left(\hat{a}_0 + \hat{b}_0\right) + \left(\hat{a}_1 + \hat{b}_1\right)(t_i - t_0) + \left(\hat{a}_2 + \hat{b}_2\right)(t_i - t_0)^2 + \hat{b}_3 (t_i - t_0)^3 + \hat{b}_4 (t_i - t_0)^4 + \sum_{j=1}^{k} \left(\hat{A}_j \sin\left(\frac{2\pi}{\hat{T}_j}(t_i - t_0) + \hat{\varphi}_j\right)\right) + \hat{B}_1 \sin\left(\frac{2\pi}{T_{\mathrm{L}}}(t_i - t_0) + \hat{\vartheta}_1\right) \tag{17}$$

The differences between the bridged (green dots in Figure 5a) and missing clocks in the gap (red dots in Figure 5a) are generally at the mm- to cm-level. For short clock gaps, the more complicated Model A does not necessarily work better than a low-order polynomial, i.e., the Model B as shown in Eq. 13. Figure 5b shows the case when Model B (with a polynomial degree of 2) is used for the clock bridging. The GRACE FO-1 satellite clock estimates over 6min from 1:58:30 to 2:04:30 (excluding the data gap from 2:00 to 2:03) on December 1, 2019, are used for the processing. Similarly, $\Delta\check{T}_{\mathrm{m}}$ is detrended in Figure 5b for better visualization. Applying Model B, the differences between the bridged and the missing clocks during the gap are reduced to millimetres.

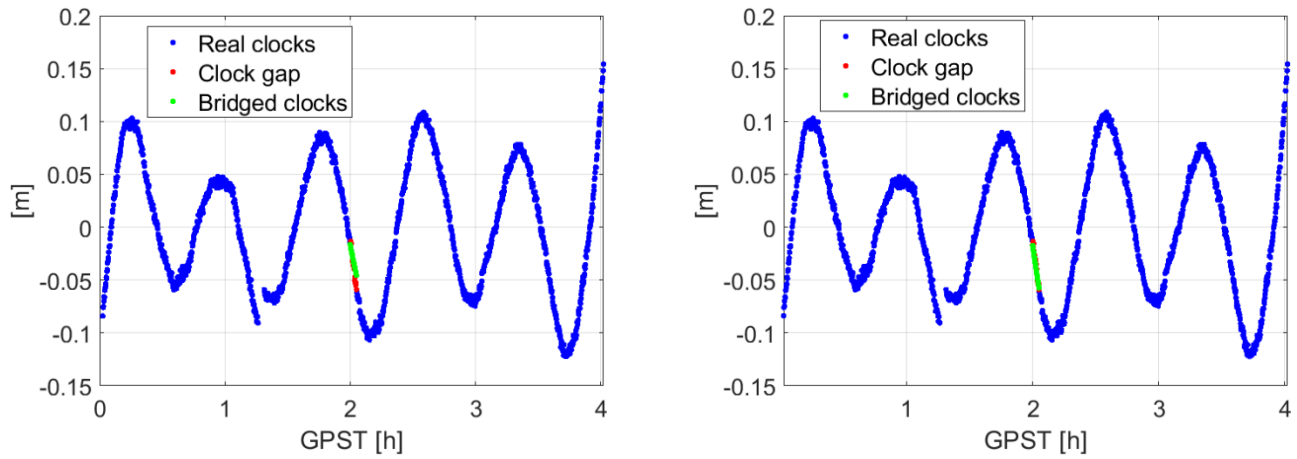

Figure 5. The real and bridged LEO satellite clocks for GRACE FO-1 on December 1, 2019, with the gap assumed from 2:00 to 2:03 GPST using (a) Model A and (b) Model B. The term $\Delta\check{T}_{\mathrm{m}}$ (Eq. 17) is detrended for better visualization.

For small clock gaps, as noted before, larger bridging errors, i.e., of the order of decimetres, could also occur when applying Model A, as the periodic behaviour of the clocks cannot be perfectly described by the suggested sinusoidal models. Figure 6 shows an example of the clocks after detrending with the term $\Delta\check{T}_{\mathrm{m}}$ (Eq. 17). The abnormal behaviours remaining in the real clocks (blue) are due not only to the miss-modelled biases in the 2/rev effects, but also from those in the 1/rev and long-term effects. As stated in [34], the 1/rev effects could be associated with external effects (such as voltage variation) in the spacecraft. The reasons for the long-term systematic effects are not clear. In addition, the mid- to long-term noise behaviour of the USO itself could also contribute to the miss-modelled bridging errors as shown in Figure 6. Hence, for small clock gaps, making use of a newly fitted low-order polynomial using the data near the clock gap, i.e., applying Models B and C, could be better options.

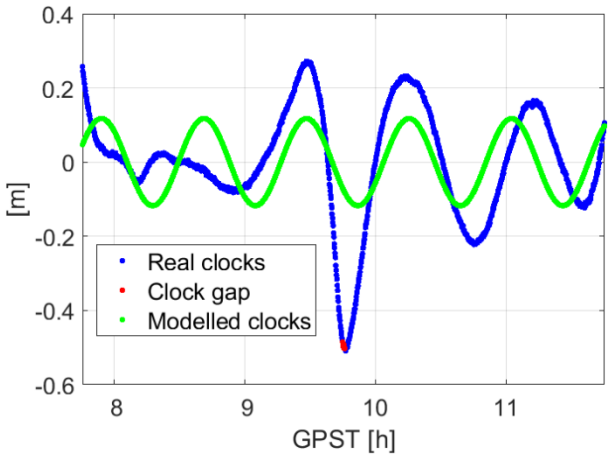

Figure 6. The real and modelled LEO satellite clocks for GRACE FO-1 on December 1, 2019, from 7:45:30 to 11:45:20 GPST, with the clock gap set between 9:45 and 9:46. The term $\Delta\check{T}_{\mathrm{m}}$ (Eq. 17) is detrended for better visualization.

For longer time gaps, the simpler Model B is not good enough to describe the systematic effects in the clocks. Figure 7a illustrates the missing and bridged clocks from 2:00 to 3:00 GPST of the test day. The term $\Delta\check{T}_{\mathrm{m}}$ (Eq. 17) is detrended for better visualization. The 4h data used for modelling the 1/rev and 2/rev effects last from 0:30:00 to 4:29:50 GPST, and the data during the 1h gap is not used. The differences between the missing (red dots in Figure 7a) and bridged clocks (green dots in Figure 7a) are generally at a few centimetres by applying Model A. Applying only a quadratic polynomial (Model B) for modelling the clocks, as shown in Figure 7b, is not good enough to describe the different systematic effects in the clocks. Using data over 2h near the gap period, i.e., from 1:30 to 3:30 excluding the gap between 2:00 and 3:00, the bridged clocks using Model B (green dots in Figure 7b) cannot follow the trend of the 1/rev effects, or even that of the long-term periodic effects. Much larger errors can result in the bridged clocks (see the

green and red dots in Figure 7b). Note that the same term $\Delta\check{T}_{\mathrm{m}}$ is detrended in Figure 7b for improved visualization, which does not mean that the periodic effects in $\Delta\check{T}_{\mathrm{m}}$ are considered in Model B. In such cases, modelling the systematic effects, i.e., applying Models A or C, becomes necessary.

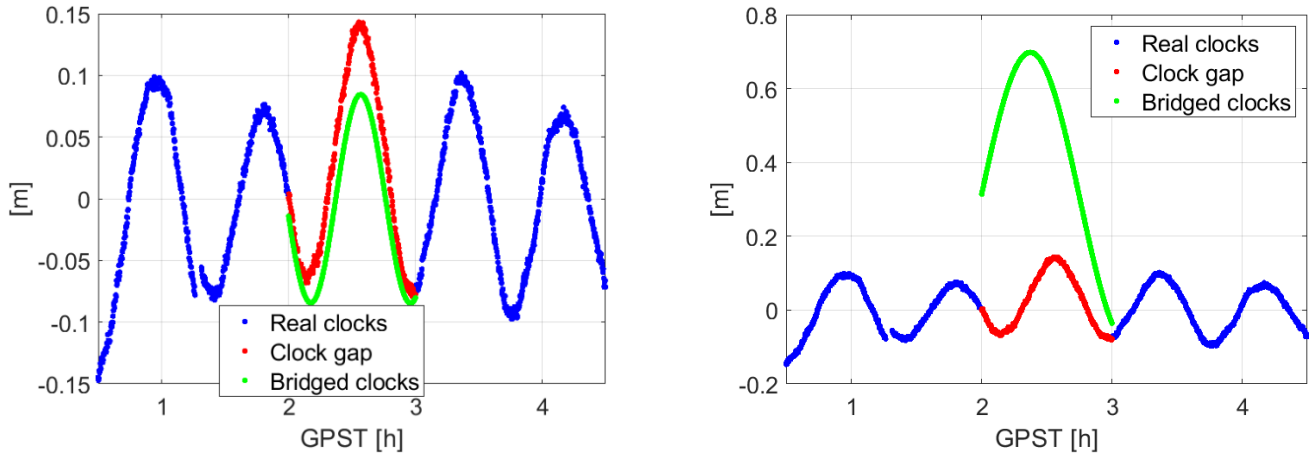

Figure 7. The real and bridged LEO satellite clocks for GRACE FO-1 on December 1, 2019, with the gap set from 2:00 to 3:00 GPST using (a) Model A and (b) Model B. The term $\Delta\check{T}_{\mathrm{m}}$ (Eq. 14) is detrended for improved visualization.

Applying the three models, the satellite clock estimates of GRACE FO-1 on December 1, 2019, are bridged for gaps with a length varying from 60s to 1h with a step of 60s. For each gap length, the gap window shifts from 2:00 to 22:00 GPST of the test day with a step of 60s, allowing a sample number of at least more than 1140 for the test of each gap length. For consistency, the LEO clock estimates used for estimation of the model coefficients all originate from the 24h daily POD process as described in the second section above "PROCESSING OF LEO SATELLITE CLOCKS".

Figure 8 shows the mean absolute bridging errors for clock gaps with a length varying from 30s to 1h. The blue, red and green lines correspond to the mean absolute bridging errors when applying Models A, B and C, respectively, while the term m in the legend denotes the polynomial degree (see Eqs. 14 and 16). It can be observed that for small clock gap periods, i.e., shorter than about 40min, Models B and C tend to have smaller bridging errors than Model A, while for longer clock gaps, Models A and C outperform Model B, which doesn't consider systematic effects at all. Model C (green lines) exploits the benefits of both Models A and B, i.e., delivering small bridging errors for short clock gaps, and having the bridging errors under control for long clock gap periods up to 1h. Having the polynomial degree increased from 2 (solid lines) to 3 (dashed lines), a slight decrease of the bridging errors can be observed for Models B and C, although with the number of unknown coefficients increased by 1.

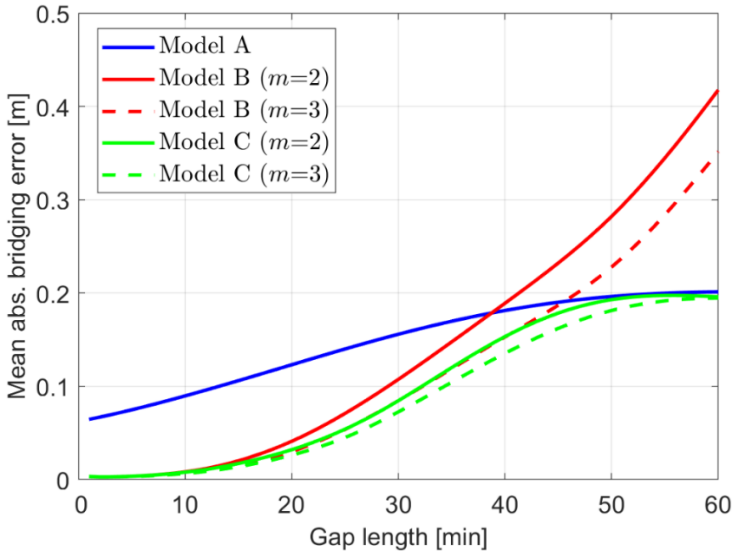

Figure 8. Mean absolute bridging errors of the LEO satellite clocks using the data of GRACE FO-1 on December 1, 2019. The red and green solid lines correspond to a quadratic polynomial, while the red and green dashed lines correspond to a cubic (third-order) polynomial.

The mean absolute bridging errors are given in Table 1 for gap lengths varying from 1 to 60min applying the three models using the data of GRACE FO-1 on December 1, 2019. It can be observed that for a short gap length less than 40min, Models B and C generally behave better than Model A, while for longer gap lengths, up to 1h, Model B shows deficiencies due to its ignorance of the systematic effects. In general, Model C is the best option among the three models, which delivers a mean absolute bridging error within 1cm for gap lengths shorter than 10min, and a mean absolute error not exceeding 0.2m even with a clock gap of 1h. Increasing the polynomial degree from two to three for Models B and C could slightly reduce the mean absolute bridging errors, i.e., with a reduction down to the mm- to cm-level.

Table 1. Mean absolute bridging errors applying Models A, B and C for different gap lengths.

Gap length [min]	Model A [m]	Model B [m]		Model C [m]	
		m=2	m=3	m=2	m=3
1	0.065	0.003	0.003	0.003	0.003
5	0.075	0.004	0.003	0.004	0.003
10	0.090	0.008	0.007	0.008	0.007
20	0.123	0.041	0.030	0.032	0.026
30	0.156	0.107	0.085	0.085	0.073
40	0.181	0.189	0.153	0.153	0.135
50	0.196	0.282	0.228	0.193	0.181
60	0.201	0.418	0.351	0.196	0.195

CONCLUDING REMARKS

Mega-constellation LEO satellites are proposed as a promising strategy to improve positioning precision, efficiency and availability for ground-based PNT users, especially when operating in difficult measurement environments. Similar to GNSS-based positioning, high-precision orbital and clock products of the LEO satellites are necessary to realize the benefits of using LEO satellites to support diverse high-precision PNT services. During the signal reception, storage and transmission processes, there are possibilities that the GNSS data used for the LEO POD and clock estimation process cannot be fully collected by a ground analysis centre, which results in gaps in the time series of clock error estimates. Even during the transmission of the clock corrections through, e.g., satellite link, signal blockage could also occur, which also results in clock gaps.

In contrast to the atomic clocks used in the GNSS satellites, the LEO satellites may use Ultra-Stable Oscillators (USOs), which exhibit different noise behaviour, especially over the long-term. Taking the USOs onboard the LEO satellite GRACE FO-1 as an example, mid- to long-term systematic behaviours exist due to the unmodelled relativistic effects and possibly other external influences. This study proposes three models for bridging the time series gaps in the USOs installed on LEO satellites: Model A considers the mid- to long-term systematic effects, Model B bridges the gap with low-order polynomial using the data nearby, and Model C exploits the benefits of both the Models A and B. Tests have demonstrated that for bridging short clock gaps up to about 40min, Models B and C are better options, while Models A and C are shown to behave better for bridging longer clock gaps up to 1h. Applying Model C, using real data of GRACE FO-1, the mean absolute bridging errors are shown to be within 1cm for gaps shorter than 10min, and are within 0.2m for gaps up to 1h. Increasing the polynomial degree from 2 to 3 did lead to a slight reduction in the bridging errors down to the mm- to cm-level.

ACKNOWLEDGMENTS

This work is funded by the Australian Research Council Discovery Project (DP190102444): Tracking Formation-Flying of Nanosatellites Using Inter-Satellite Links, the National Time Service Center, Chinese Academy of Sciences (CAS) (No. E167SC14), and the CAS "Light of West China" Program (No. XAB2018YDYL01).

REFERENCES

1. Reid, T. G. R., Neish, A. M., Walter, T., and Enge, P. K., "Broadband LEO constellations for navigation," *Navigation, Journal of the Institute of Navigation*, Vol. 65, Issue 2, 2018, pp. 205–220. doi: 10.1002/navi.234
2. Ge, H., Li, B., Ge, M., Zang, N., Nie, L., Shen, Y., and Schuh, H., "Initial assessment of precise point positioning with LEO enhanced global navigation satellite systems (LeGNSS)," *Remote Sensing*, Vol. 10, Issue 7, 2018, 984. doi: 10.3390/rs10070984
3. Li, X., Ma, F., Li, X., Lv, H., Bian, L., Jiang, Z., and Zhang, X., "LEO constellation-augmented multi-GNSS for rapid PPP convergence," *Journal of Geodesy*, Vol. 93, 2018, pp. 749-764. doi: 10.1007/s00190-018-1195-2
4. Han, Y., Wang, L., Fu, W., Zhou, H., Li, T., Xu, B., and Chen, R., "LEO navigation augmentation constellation design with the multi-objective optimization approaches," *Chinese Journal of Aeronautics*, 2020, Vol. 34, Issue 4, pp. 265-278. doi: 10.1016/j.cja.2020.09.005
5. Lawrence, D., Cobb, H. S., Gutt, G., O'Connor, M., Reid, T. G. R., Walter T., and Whelan, D., "Innovation: Navigation from LEO," *GPS World*, June 30, 2017. Accessed on March 27, 2021 at https://www.gpsworld.com/innovation-navigation-from-leo/
6. Faragher, R., and Ziebart, M., "OneWeb LEO PNT: Progress or Risky Gamble?" *Inside GNSS*, September 28, 2020. Accessed on June 28, 2021 at https://insidegnss.com/oneweb-leo-pnt-progress-or-risky-gamble/
7. Ge, H., Li, B., Ge, M., Zang, N., Nie, L., Shen, Y., and Schuh, H., "Initial assessment of precise point positioning with LEO enhanced global navigation satellite systems (LeGNSS)," *Remote Sensing*, Vol. 10, Issue 7, 2018, 984. doi: 10.3390/rs10070984
8. Li, X., Ma, F., Li, X., Lv, H., Bian, L., Jiang, Z., and Zhang, X., "LEO constellation-augmented multi-GNSS for rapid PPP convergence," *Journal of Geodesy*, Vol. 93, 2018, pp. 749-764. doi: 10.1007/s00190-018-1195-2
9. Montenbruck, O., Gill, E., and Kroes, R., "Rapid orbit determination of LEO satellites using IGS clock and ephemeris products," *GPS Solutions*, Vol. 9, 2005, pp. 226–235. doi: 10.1007/s10291-005-0131-0
10. Wang K., Allahvirdi-Zadeh A., El-Mowafy A., and Gross J., "A sensitivity study of POD using dual-frequency GPS for CubeSats data limitation and resources," *Remote Sensing*, Vol. 12, Issue 13, 2020, 2107. doi:10.3390/rs12132107
11. Gu, D., Ju, B., Liu, J., and Tu, J., "Enhanced GPS-based GRACE baseline determination by using a new strategy for ambiguity resolution and relative phase center variation corrections," *Acta Astronautica*, Vol. 138, 2017, pp. 176–184. doi: 10.1016/j.actaastro.2017.05.022
12. Wang K., and El-Mowafy A., "LEO satellite clock analysis and prediction for positioning applications," *Geo-spatial information science*, 2021, doi:10.1080/10095020.2021.1917310
13. Wang, L., Chen, R., Li, D., Zhang, G., Shen, X., Yu, B., Wu, C., Xie, S., Zhang, P., Li, M., and Pan, Y. "Initial assessment of the LEO based navigation signal augmentation system from Luojia-1A satellite," *Sensors*, Vol. 18, Issue 11, 2018, 3919. doi: 10.3390/s18113919

14. Johnston, G., Riddell, A., and Hausler, G., "The International GNSS Service," In: Teunissen PJG, Montenbruck O (eds) *Springer Handbook of Global Navigation Satellite Systems*, 2017, Springer Handbooks. Springer, Cham, Switzerland. pp. 967–982. doi:10.1007/978-3-319-42928-1_33
15. El-Mowafy, A., Deo, M., and Kubo, N., "Maintaining real-time precise point positioning during outages of orbit and clock corrections," *GPS Solutions*, Vol. 21, 2017, pp. 937-947. doi:10.1007/s10291-016-0583-4
16. Hadas, T., and Bosy, J., "IGS RTS precise orbits and clocks verification and quality degradation over time," *GPS Solutions*, Vol. 19, 2015, 93–105. doi: 10.1007/s10291-014-0369-5
17. Laurichesse, D., Cerri, L., Berthias, J. P., and Mercier, F., "Real time precise GPS constellation and clocks estimation by means of a Kalman filter," *Proceedings of the 26th International Technical Meeting of the Satellite Division of The Institute of Navigation (ION GNSS+ 2013), Nashville, TN, USA, September 2013*, pp. 1155–1163.
18. El-Mowafy, A., and Wang, K., (2019) "Second Generation SBAS – Performance Analysis and Bridging Positioning and Integrity Monitoring during SBAS Outages in the Urban Environment," *Proceedings of the 32nd International Technical Meeting of the Satellite Division of The Institute of Navigation (ION GNSS+ 2019*), *Miami, Florida, USA, September 2019*, pp. 2842-2854. doi: 10.33012/2019.16923
19. Montenbruck, O., and Gill, E., "Around the world in a hundred minutes," In *Satellite orbits*, 1st ed.; Springer: Berlin, Heidelberg, Germany, 2000, pp. 1–13.
20. Allahvirdi-Zadeh, A., Wang, K., and El-Mowafy, A., "POD of small LEO satellites based on precise real-time MADOCA and SBAS-aided PPP corrections," *GPS Solutions*, Vol. 25, 2021, 31. doi: 10.1007/s10291-020-01078-8
21. Dach, R., Lutz, S., Walser, P., Fridez, P., "Bernese GNSS Software Version 5.2," Astronomical Institute, University of Bern, Bern, Switzerland, 2015.
22. Weinbach, U., and Schön S., "Improved GPS receiver clock modeling for kineamtic orbit determination of the GRACE satellites," *Proceedings of the 2012 European Frequency and Time Forum (EFTF), Gothenburg, Sweden, April 2012*. doi: 10.1109/EFTF.2012.6502356
23. Ko, U. D., and Tapley, B. D., "Computing the USO frequency instability of GRACE satellites," *Proceedings of the 2010 IEEE Aerospace Conference, Big Sky, MT, USA, March 2010*. doi: 10.1109/AERO.2010.5446732
24. Case, K., Kruizinga, G., and Wu, S. C., "GRACE Level 1B data product user handbook," Jet Propulsion Laboratory, California Institute of Technology, JPL D-22027, March 24, 2010.
25. Wen, H. Y., Kruizinga, G., Paik, M., Landerer, F., Bertiger, W., Sakumura, C., Bandikova, T., and Mccullough, C., "Gravity Recovery and Climate Experiment Follow-On (GRACE-FO) Level-1 data product user handbook," Jet Propulsion Laboratory, California Institute of Technology, JPL D-56935, September 11, 2019.
26. ESA, "SENTINEL-3, ESA's Global Land and Ocean Mission for GMES Operational Services," European Space Agency. SP-1322/3, October 2012.
27. Dach, R., Brockmann, E., Schaer, S., Beutler, G., Meindl, M., Prange, L., Bock, H., Jäggi, A., and Ostini, L., "GNSS processing at CODE: status report," *Journal of Geodesy*, 2009, Vol. 83, pp. 353-365. doi:10.1007/s00190-008-0281-2
28. Pavlis, N. K., Holmes, S. A., Kenyon, S. C., and Factor, J. K., "An Earth gravitational model to degree 2160: EGM2008," *European Geosciences Union General Assembly, Vienna, Austria, April 2008*.
29. Standish, E. M. "The JPL Planetary and Lunar Ephemerides," DE405/LE405, 1998, JPL IOM 312, F-98-048.
30. Petit, G., and Luzum, B. "IERS Conventions. IERS Technical Note, 36," Verlag des Bundesamts für Kartographie und Geodäsie, Frankfurt am Main, Germany, 2010. 179p, ISBN: 3-89888-989-6
31. Lyard, F., Lefevre, F., Letellier, T., and Francis, O. (2006) "Modelling the global ocean tides: modern insights from FES2004," *Ocean Dynamics*, 2006, Vol. 56, pp. 394–415. doi: 10.1007/s10236-006-0086-x
32. Montenbruck, O., and Gill, E., "Satellite Orbits: Models, Methods and Applications," Springer, Berlin, Heidelberg, Germany, 2000. doi:10.1007/978-3-642-58351-3
33. Wen, H. Y., Kruizinga, G., Paik, M., Landerer, F., Bertiger, W., Sakumura, C., Bandikova, T., and Mccullough, C., "Gravity Recovery and Climate Experiment Follow-On (GRACE-FO) Level-1 Data Product User Handbook," JPL D-56935 (URS270772), NASA Jet Propulsion Laboratory, California Institute of Technology, September 11, 2019.
34. Larson KM, Ashby N, Hackman C, Bertiger W (2007) An assessment of relativistic effects for low Earth orbiters: the GRACE satellites. Metrologia, 44(6): 484-490. doi: 10.1088/0026-1394/44/6/007